Observed Atlantification of the Barents Sea Causes the Polar Front to Limit the Expansion of Winter Sea Ice

BENJAMIN I. BARTON

Laboratoire d'Océanographie Physique et Spatiale, UMR 6523, CNRS-Ifremer-UBO-IRD, Brest, France

YUENG-DJERN LENN

School of Ocean Sciences, Bangor University, Bangor, United Kingdom

CAMILLE LIQUE

Laboratoire d'Océanographie Physique et Spatiale, UMR 6523, CNRS-Ifremer-UBO-IRD, Brest, France

(Manuscript received 8 January 2018, in final form 21 June 2018)

ABSTRACT

Barents Sea Water (BSW) is formed from Atlantic Water that is cooled through atmospheric heat loss and freshened through seasonal sea ice melt. In the eastern Barents Sea, the BSW and fresher, colder Arctic Water meet at the surface along the Polar Front (PF). Despite its importance in setting the northern limit of BSW ventilation, the PF has been poorly documented, mostly eluding detection by observational surveys that avoid seasonal sea ice. In this study, satellite sea surface temperature (SST) observations are used in addition to a temperature and salinity climatology to examine the location and structure of the PF and characterize its variability over the period 1985–2016. It is shown that the PF is independent of the position of the sea ice edge and is a shelf slope current constrained by potential vorticity. The main driver of interannual variability in SST is the variability of the Atlantic Water temperature, which has significantly increased since 2005. The SST gradient associated with the PF has also increased after 2005, preventing sea ice from extending south of the front during winter in recent years. The disappearance of fresh, seasonal sea ice melt south of the PF has led to a significant increase in BSW salinity and density. As BSW forms the majority of Arctic Intermediate Water, changes to BSW properties may have far-reaching impacts for Arctic Ocean circulation and climate.

1. Introduction

The Arctic has been predicted to be free of sea ice in summer by the middle of the twenty-first century (Wang and Overland 2012; Snape 2013; Notz and Stroeve 2016). This follows an Arctic-wide decline in sea ice extent over recent decades (Screen and Simmonds 2010). The Barents Sea alone has seen a 50% reduction in annual sea ice area between 1998 and 2008 (Årthun et al. 2012), associated with a strong sea ice decline in all seasons including winter (Onarheim and Årthun 2017). Seasonal sea ice extent variations are very predictable in the Barents Sea compared with other parts of the Arctic (Sigmond et al. 2016). For instance, Day et al. (2014) found significant correlations between Arctic sea ice extent in May and Barents Sea sea surface temperature (SST) for the same month, as well as with SST in the preceding December. The variability of the Barents Sea ice edge location has also been associated with atmospheric circulation (Sorteberg and Kvingedal 2006) and ice exported from the Arctic to the Barents Sea due to local winds (Koenigk et al. 2009; Kwok 2009). On longer time scales, the reduction in annual and winter sea ice area in the Barents Sea is thought to be driven by an increase in the heat transport into the Barents Sea due to the combined increase in advection and temperature of Atlantic Water (AW; Årthun et al. 2012; Onarheim et al. 2015). AW temperature and salinity in the Barents Sea are also varying on multidecadal time scales (Levitus et al. 2009; Smedsrud et al. 2013), making it challenging to distinguish between long-term trends and natural variability.

Along with Fram Strait, the Barents Sea Opening (BSO) is a gateway for the warm and salty AW (defined

Corresponding author: Benjamin I. Barton, benjamin.barton@univ-brest.fr

DOI: 10.1175/JPO-D-18-0003.1

TABLE 1. Definitions of the water masses present in the Barents Sea used in this study, along with definitions used in previous studies. Note that Barents Sea Water can be referred to as Modified Atlantic Water in literature.

Water mass	Source	Temperature (°C)	Salinity (PSU)	Density ($\rho - 1000\,\mathrm{kg\,m^{-3}}$)
Atlantic Water (AW)	Present study	$T > 3.0$	$S > 35.0$	
	Oziel et al. (2016)	$T > 3.0$	$S > 34.8$	
	Loeng (1991)	$T > 3.0$	$S > 35.0$	
Arctic Water (ArW)	Present study	$T < 0.0$	$S < 34.7$	
	Oziel et al. (2016)	$T < 0.0$	$S < 34.7$	
	Loeng (1991)	$T < 0.0$	$34.3 < S < 34.8$	
Coastal Water (CW)	Present study	$T > 2.0$	$S < 34.7$	
	Oziel et al. (2016)	$T > 3.0$	$S < 34.4$	
	Loeng (1991)	$T > 2.0$	$S < 34.7$	
Barents Sea Water (BSW)	Present study	$T < 2.0$	$S > 34.7$	$\sigma > 27.85$
	Schauer et al. (2002)			$\sigma > 27.85$
	Oziel et al. (2016)	$T < 2.0$	$S > 34.8$	$\sigma > 27.8$
	Loeng (1991)	$-1.5 < T < 2.0$	$34.7 < S < 35.0$	

in Table 1) entering the Arctic Ocean and its marginal seas (Fig. 1). The branch of AW entering through the BSO transits the Barents Sea, where it is modified en route, forming Barents Sea Water (BSW; Table 1; Schauer et al. 2002; Harris et al. 1998). This transformation into BSW is driven mainly by surface interactions with the atmosphere resulting in winter convection and entrainment of freshwater. Heat is lost from the ocean through turbulent heat flux and longwave radiation (Long and Perrie 2017), while freshwater input mostly comes from seasonal sea ice import and rivers (Ellingsen et al. 2009). Thus, the length and location of the pathway along which AW flows determines to what extent its properties are modified by surface fluxes, sea ice, and rivers before it enters the Arctic basin. The Barents Sea bathymetry is known to strongly influence the path of AW inflow (Fig. 1; Loeng 1991). Part of the AW inflow crosses Murmansk Rise, south of Central Bank, into the Central Basin (Skagseth 2008; Ingvaldsen 2005). The Central Basin acts as a reservoir for AW until it loses enough buoyancy to propagate northward below Arctic Water (ArW) as BSW. As a result, the water column is stratified in the northern Barents Sea, with the upper 100 m occupied by relatively fresh and cold ArW (Table 1) and the lower layer occupied by BSW (Harris et al. 1998; Lind and Ingvaldsen 2012).

In situ observations in the western Barents Sea have revealed that the surface expression of the front separating AW from ArW follows isobaths in the range of 150–275 m (Gawarkiewicz and Plueddemann 1995; Harris et al. 1998; Våge et al. 2014; Fer and Drinkwater 2014). In the eastern Barents Sea, the northern front [referred to as the Polar Front (PF) hereafter] is defined as the location where BSW meets ArW, but its geographic position is poorly defined (Oziel et al. 2016). The PF is a water mass boundary and therefore should have an SST signature. This PF should be distinguished from another nearby SST front (hereafter thermal-surface front) that is also expected to be present in the surface layer of the northern Barents Sea following the sea ice edge, due to the transition from freezing-point water to ice-free water. In the range of the temperatures and salinities of BSW and ArW, salinity and temperature tend to contribute equally to the determination of density (Parsons et al. 1996; Våge et al. 2014). Thus, both surface temperature and surface salinity contribute to the PF's surface density gradient, suggesting that the variability of the PF position can be influenced by other processes than just the position of the sea ice edge.

BSW exits the Barents Sea, entering the Arctic Ocean mainly through St. Anna Trough (Rudels et al. 2000; Smedsrud et al. 2013). In the Arctic Ocean, BSW is entrained into Arctic Intermediate Water (AIW), accounting for 50%–80% of the volume of AIW (Schauer et al. 1997; Maslowski et al. 2004). AIW is ultimately exported to the North Atlantic through Fram Strait and in turn contributes to the deeper branch of the Atlantic meridional overturning circulation (AMOC; Aagaard et al. 1985; Fahrbach et al. 2001). There is some debate in the literature about the extent to which BSW properties at the exit of the Barents Sea are preserved into the Arctic Ocean and beyond. Observations have revealed that some mixing of BSW occurs on continental slopes and within the Arctic Ocean (Shapiro 2003; Rudels et al. 2015), but model results of Lique et al. (2010) show modifications to BSW properties within the Arctic Ocean are small compared to the modification within the Barents Sea. In either case, the properties with which BSW exits the Barents Sea are important as they precondition it for the target depth at which it may settle and mix with ambient water masses within the Arctic basin. Anomalies in BSW density have been traced to Denmark

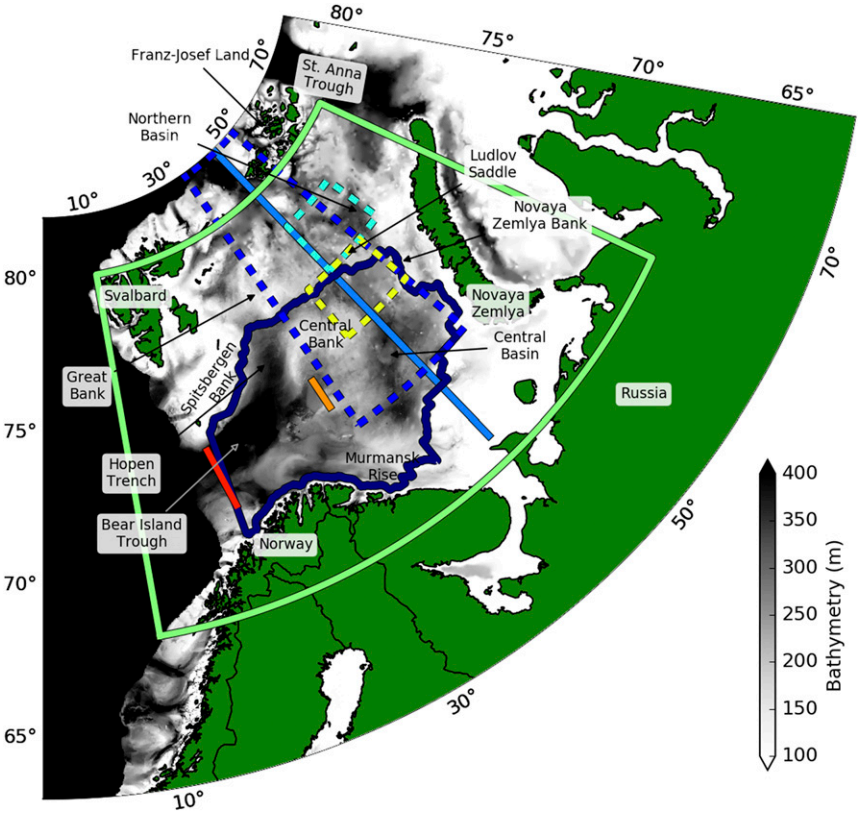

FIG. 1. Bathymetry of the Barents Sea. The different lines and boxes indicate the area used for EOF analysis of SST (green box), the region used for Hovmöller analysis (blue dashed box), the cross-front transect (light-blue line), the area selected for calculating the contribution of sea ice to AW/BSW (dark-blue box), the area selected for 100–300-m BSW properties from EN4 data and 0–100-m ArW properties from EN4 data (cyan dashed box), the area selected for 0–100-m surface BSW properties from EN4 data south of the PF (yellow dashed line), the Kola section (orange line), and the Fugløya–Bear Island section (red line).

Strait, suggesting far-reaching impacts from processes occurring in the Barents Sea (Karcher et al. 2011).

It has been hypothesized by Aagaard and Woodgate (2001) that a prolonged reduction in the fresh, meltwater input from seasonal sea ice into BSW could cause a modification of the BSW properties, and in turn induce a warming and salinification of AIW. This hypothesis overlooks the role the PF could play in determining whether the meltwater is entrained into BSW or ArW and discounts the influence of changes in other water masses in the Barents Sea. Indeed, both the transport and the temperature of AW circulating in the Barents Sea have increased in recent decades (Årthun et al. 2012), resulting in a reduction in winter sea ice area through a decrease in wind-driven sea ice advection and delayed winter refreezing (Lien et al. 2017). Thus, winter sea ice extent trends are consistent with the emerging evidence of ongoing Atlantification (i.e., the increased influence of AW resulting in a warming and salinification) of the Barents Sea (Reigstad et al. 2002; Oziel et al. 2017) and Arctic Ocean (Polyakov et al. 2017). This makes it important to quantify the role that Barents Sea ice trends play on BSW properties.

The goal of this study is to investigate the variability of SST in order to characterize the PF's location in the eastern Barents Sea and to determine how this compares to the seasonal sea ice edge and what the implications for BSW formation are, given the documented sea ice loss and Atlantification of the Barents Sea. To that aim, we use a combination of the new, high-resolution, 32-yr Operational Sea Surface Temperature and Sea Ice Analysis (OSTIA) SST dataset, satellite observations of sea ice concentration, and 3D optimally interpolated temperature and salinity products.

The methods and tools are presented in section 2. To identify forcings on the formation of BSW, in section 3 the mechanisms that cause variability in SST on seasonal and to multidecadal time scales in the Barents Sea are explored. In section 4, SST is used to pinpoint the

surface expression of the PF and determine whether the winter sea ice edge has become bound by it. In section 5, the results of sections 3 and 4 are brought together and the consequences of a regime shift for BSW properties are discussed. Conclusions are presented in section 6.

2. Data and methods

a. Datasets

This study makes use of satellite SST and sea ice concentration data from the OSTIA project spanning from January 1985 to December 2016 (Donlon et al. 2012; downloaded from http://marine.copernicus.eu/). This dataset is optimally interpolated from multiple satellite sensors together with in situ observations onto a 0.05° grid (1.5 km × 5.6 km for the Barents Sea) at a daily frequency. The feature resolution is 10 km and the accuracy of the daily data is ~0.57 K (Donlon et al. 2012). At the current spatial and temporal resolution, the satellite SST data used in this study cannot yet resolve mesoscale variability (with a characteristic scale of only a few kilometers) in the Barents Sea. Sea ice extent in the Barents Sea is computed from the OSTIA sea ice concentration. The sea ice edge is defined as the 15% contour of the sea ice concentration.

Bathymetry is taken from the General Bathymetric Chart of the Oceans (GEBCO) 2014 30-arc-s-resolution dataset (Weatherall et al. (2015); GEBCO_2014 Grid, version 20150318, www.gebco.net). In the Barents Sea, it corresponds to a resolution of 0.2 km in longitude and 0.9 km in latitude. We also use fields of surface air temperature (SAT; corresponding to temperature at 2 m above surface) and sea level pressure (SLP) from the ECMWF ERA-Interim reanalysis (Berrisford et al. 2011; www.ecmwf.int). This dataset is provided on a 0.75° grid (84 km × 16 km for the Barents Sea) with 3-hourly temporal resolution, averaged into monthly means.

Observations from the Fugløya–Bear Island section along 20.0°E in the BSO (red line, Fig. 1) are used to characterize the variations of the AW inflow temperature and salinity (Larsen et al. 2016). This dataset is available through the International Council for the Exploration of the Sea (ICES) portal (http://ocean.ices.dk/iroc/) and corresponds to hydrographic profiles, collected six times a year, used for the period from January 1985 to October 2015. The time series presented here is averaged over the 50–200 m depth range and between 71.5° and 73.5°N (Ingvaldsen et al. 2003), and is thus representative of the subsurface temperature and salinity variability. We also use observations from the Kola section (available through www.pinro.ru), extending from 73.0° to 74.0°N along 33.5°E (orange line, Fig. 1), as a proxy for the AW temperature in the central Barents Sea. Along the section, conductivity–temperature–depth (CTD) profiles have been collected between 7 and 9 times per year, and we use the subset from January 1985 to December 2015 (Bochkov 1982; Ingvaldsen et al. 2003). We consider again the depth range between 50 and 200 m (i.e., the subsurface), which is below the depth of the summer mixed layer and is the depth range over which the core of AW enters the Barents Sea (Ingvaldsen 2005).

To examine the variability and long-term trends over the wider region than just these two sections, temperature and salinity fields from the EN4 dataset are analyzed (EN4.2.0, www.metoffice.gov.uk/hadobs/en4). EN4 comprises in situ ship CTD profile data and Argo float data optimal interpolated on a 1°, monthly z grid with 42 levels (Gouretski and Reseghetti 2010). Data used in this analysis are from the January 1985 to December 2016 period. Between 1985 and 2015, there is a minimum of two profiles of temperature and salinity per year in the northeastern Barents Sea. It should be noted that there is a summer bias in this dataset based on when most of the ship-based profiles were collected. To accommodate the variability in profile sampling, the uncertainty values provided in EN4 are considered throughout this study (Good et al. 2013).

Additional temperature and salinity fields are retrieved from the Monthly Isopycnal/Mixed-Layer Ocean Climatology (MIMOC) ocean climatology project (www.pmel.noaa.gov/mimoc), which optimally interpolates in situ ship CTD profiles and Argo float data onto a 0.5° σ grid followed by an 81-level z grid (Schmidtko et al. 2013). The monthly climatology is weighted to be representative of 2007–11. MIMOC data were included in this study as their higher spatial resolution allows a better description of the 3D structure of the front than EN4 data, although they do not provide information on the interannual variations of the fields.

b. Methods

The Barents Sea SST seasonal climatology is calculated from the OSTIA data. To resolve the PF, the magnitude of the gradient in SST for both the latitude and longitude directions are calculated using the equation $|\nabla T_{(x,y)}| = \sqrt{(\partial T/\partial x)^2 + (\partial T/\partial y)^2}$.

To characterize the temporal and spatial variability in SST over the Barents Sea, empirical orthogonal functions (EOFs) are calculated using the singular value decomposition (SVD) method (Thomson and Emery 2014). EOF analysis extracts the main mode of SST interannual variability, providing us with a spatial pattern and an associated time-varying index referred to as the principal component (PC). The area selected for EOF analysis covers the Barents Sea (10°–65°E and 68°–80°N; see green box, Fig. 1). Prior to the EOF decomposition

several steps were taken. These are 1) data points within 28 km (5 grid cells) of land were removed as well as the Kara Sea and any isolated inlets with restricted connectivity to the Barents Sea that would be unrepresentative of the variability in the Barents Sea; 2) the seasonal cycle was then removed from the SST monthly means in each grid cell by applying a 12-month running mean to the data; 3) the mean SST at each grid cell was then removed, and 4) finally, SST in each grid cell was divided by its respective standard deviation. We also compute correlations between the PC and other fields that were also subject to a 12-month running mean.

A two-tailed Welch's t test is used to estimate the significance of a difference between two given time periods, while a two-tailed Student's t test is used for the significance of linear trends in monthly SST. For estimating the 95% level significance of correlations, a two-tailed Student's t test is used and an appropriate reduction in degrees of freedom associated with a 12-month running mean is accounted for.

In this study, the criteria used to define the different water masses mostly follow previous definitions found in the literature (e.g., Loeng 1991; Table 1). The main adjustment made to existing definitions is the minimum density set for the BSW definition ($\sigma > 27.85\,\mathrm{kg\,m^{-3}}$); it ensures that we reject the warm and fresh surface water that is not dense enough to sink into the Arctic Ocean. Note that our results are mostly insensitive to the exact definition of the different water masses. For the EN4 and MIMOC datasets, potential density is determined using the Thermodynamic Equation of Seawater 2010 (TEOS-10; McDougall et al. 2012). Practical salinity and potential temperature are also estimated and presented throughout to allow direct comparison to results found in the literature.

To quantify the changes of the BSW properties over time, we estimate the mean BSW temperature and salinity from EN4 data within a domain in the northeastern Barents Sea (northern basin, 44°–54°E and 76.5°–78.5°N; see cyan dashed box, Fig. 1). We only consider the depth range 100–300 m, as in this region, BSW is isolated from the atmosphere by the ArW layer, inhibiting further modification before BSW reaches the Arctic basin. ArW properties are defined in the 0–100-m layer within the same region from EN4. Surface BSW properties south of the PF are defined from EN4 in the Central Basin (40°–50°E and 74.5°–76.5°N; see yellow dashed box, Fig. 1)

3. Seasonal and interannual variability of sea surface temperature in the Barents Sea

In this section, we characterize the temporal and spatial variations of SST over the Barents Sea. SST, by which the surface expression of PF is defined in section 4, is representative of air–sea interactions that are key to the formation of BSW. We first examine the seasonal cycle because this has been suggested, from model analysis, to play an important role in BSW formation (Årthun et al. 2011; Dmitrenko et al. 2014). When averaged over the Barents Sea domain (see green box in Fig. 1), the amplitude of the SST seasonal cycle amounts to 1.69°C, with minimum and maximum occurring in April and July, respectively. This value is large when compared to the standard deviation of the mean SST once the seasonal cycle is removed, which amounts to 0.41°C. Clearly, SST is dominated by seasonal variability. The annual winter reduction in SST is key to the formation of BSW through heat loss and, given this is an annual event, suggests a link between BSW and the 1–2.5-yr residence time of AW within the Barents Sea (Smedsrud et al. 2010; Årthun et al. 2011).

Maps of seasonal mean SST, over the period 2005–16, are shown in Figs. 2a–d. It reveals a pool of warm AW in the southwestern Barents Sea with a tongue of AW in the Central basin. This warm AW tongue is intensified in winter and spring but present throughout the year. In the southwestern Barents Sea, SST increases from 4°C in spring to 8°C in summer. In the remainder of the Barents Sea, the SST also increases by 4°C between spring and summer but approaches −1.8°C in the spring due to the presence of sea ice (Figs. 3a–d). The sea ice edge also shows strong seasonality, retreating to the northern margins of the Barents Sea in summer, while advancing toward Central Bank from the north and the southeast in winter. As discussed later in this section, the long-term trend in SST changes in 2005, posing the question of a possible change of SST seasonal cycle across the full period considered. The most striking difference between the 1985–2005 (Fig. 2) and the 2005–16 (Fig. 3) time periods is the location of the sea ice edge, with appreciably larger areas of open water post-2005 in all the seasons. This is accompanied by changes in SST where the seasonal sea ice has retreated.

This seasonality is primarily driven by the seasonal cycle of the net surface heat flux with a contribution from AW heat transport (Ding et al. 2016; Smedsrud et al. 2010). In the northern Barents Sea, seasonal surface heat fluxes roughly balance over a year. In contrast there is a net heat flux from ocean to atmosphere in the southern Barents Sea, suggesting the importance of heat brought here by AW for the formation of BSW (Smedsrud et al. 2010).

To examine SST variability on interannual and longer time scales, the seasonal cycle is first removed and EOF analysis is performed (see section 2 for methodology). The trend is not removed as this could be related to

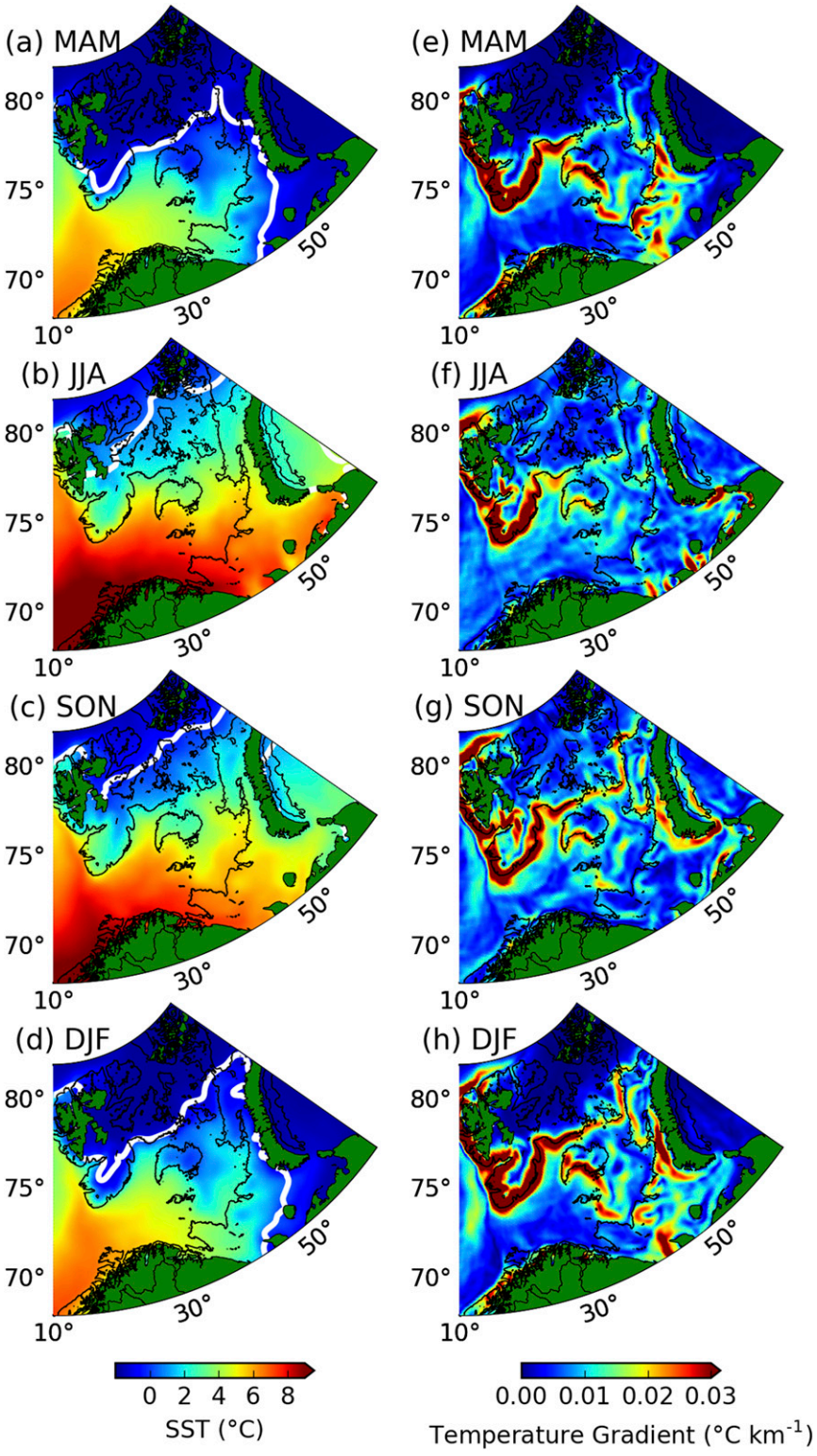

FIG. 2. (left) SST seasonal climatology and (right) gradient in SST seasonal climatology from 2005 to 2016 for (a),(e) spring (March–May), (b),(f) summer (June–August), (c),(g) autumn (September–November), and (d),(h) winter (December–February). The sea ice edge is defined by 15% sea ice concentration (white line) and the black line indicates the 220-m isobath.

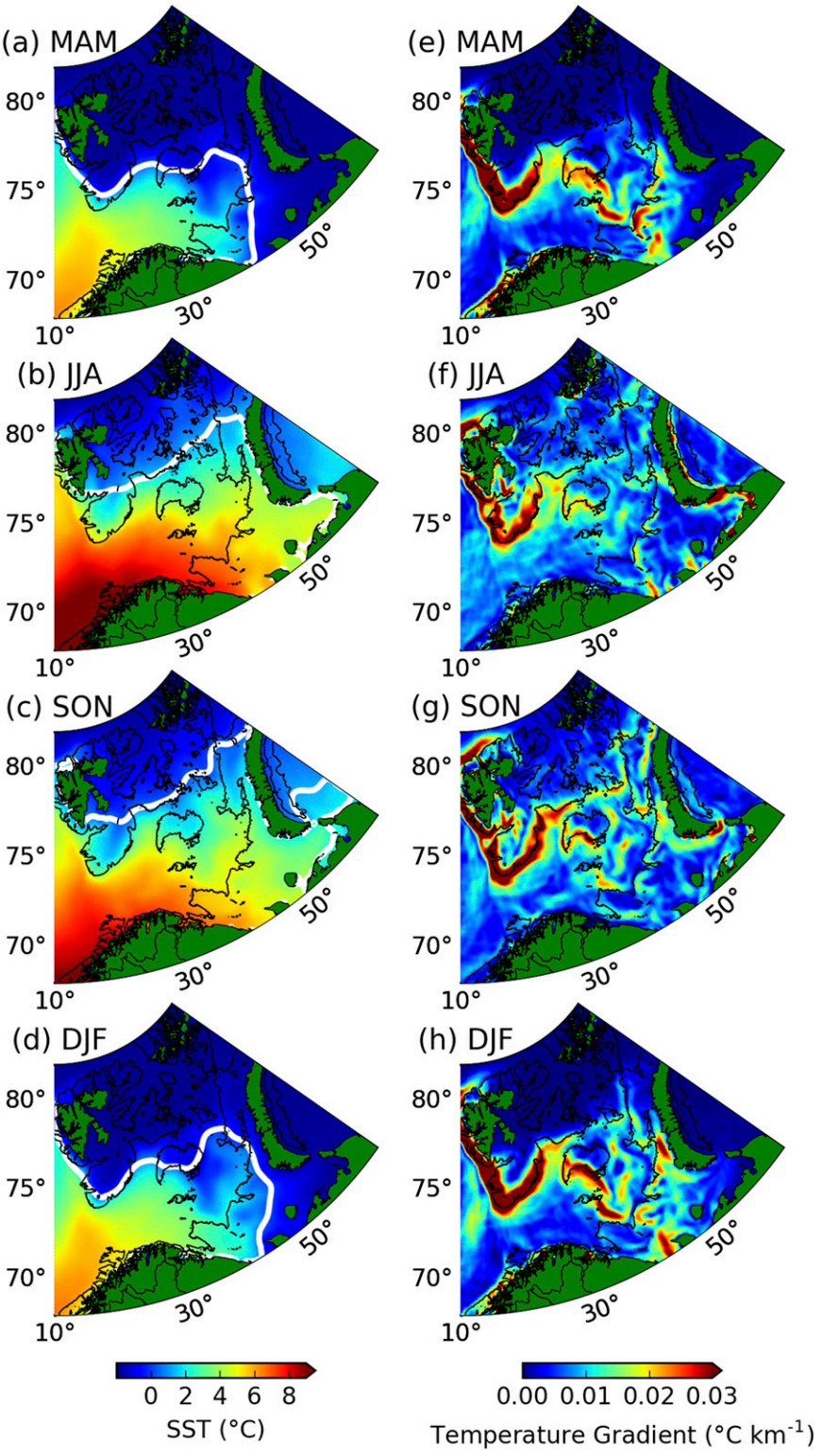

FIG. 3. As in Fig. 2, but for the seasonal climatology from 1985 to 2004.

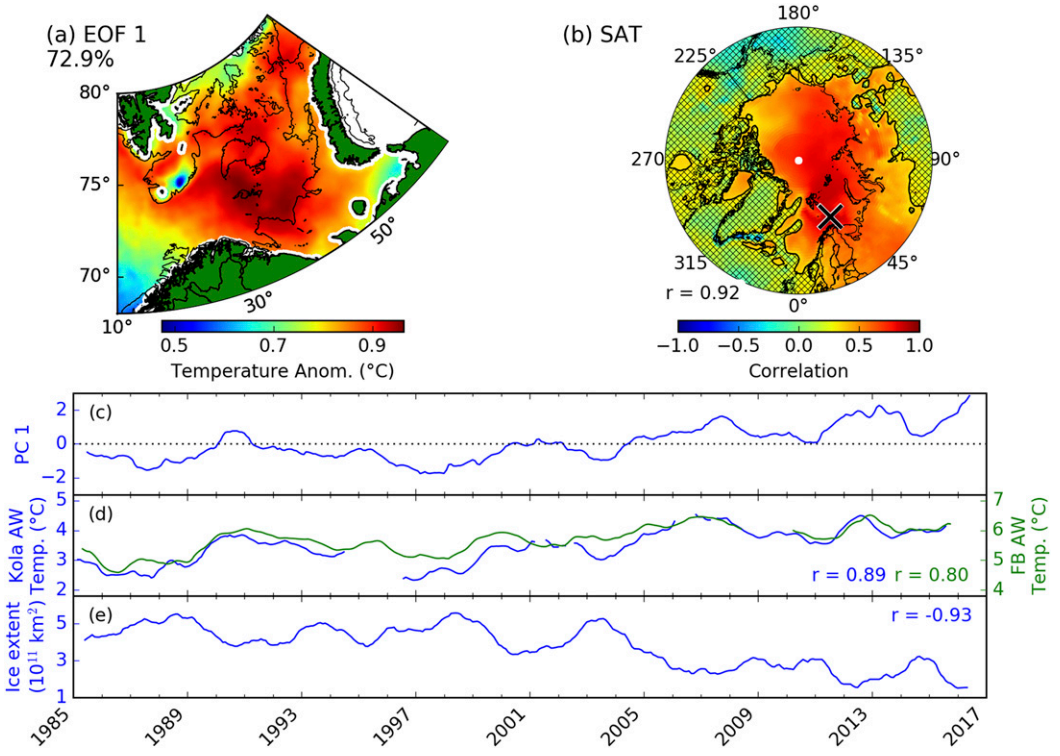

FIG. 4. (a) Spatial pattern of first EOF mode of SST variability. The black line indicates the 220-m isobath. (b) Regression of PC 1 with SAT. Maximum correlation (r value) is shown in the bottom left-hand corner, and the location of the maximum correlation is shown by a black cross. Hatched areas are not significant at the 95% level. (c) Time series of PC 1. (d) Time series of AW temperature at the Kola section (blue line, 12-month running mean applied) and Fugløya–Bear Island (FB) section (green line, 12-month running mean applied). (e) Time series of sea ice extent in the Barents Sea (12-month running mean applied). Correlations between each variable and PC 1 are indicated.

multidecadal variability discussed later in this section. The first mode (EOF1) of variability in SST explains 72.9% of the variance. As the second mode explains less than 10% of the variance, we only discuss EOF1. The spatial pattern of EOF1 is a positive anomaly across the full Barents Sea (Fig. 4a). PC1 has a periodicity of 6–10 years but also exhibits multidecadal variability (Fig. 4c). PC1 is strongly correlated with the interannual variations of SAT over the Barents Sea where SAT leads by 2 months (Fig. 4b). Regressing PC1 on the SAT fields reveals an area of significant positive correlation over the Arctic Ocean, eastern Arctic shelf seas, and northern Russia. Lag correlations with AW temperature show AW leads SST by 2–4 months. PC1 is significantly correlated with the variation of AW temperature at the Kola section ($r = 0.89$, lag $= -2$ months; Fig. 4d) and the Fugløya–Bear Island section ($r = 0.80$, lag $= -4$ months; Fig. 4d). PC1 is also anticorrelated with the variations of the sea ice extent in the Barents Sea ($r = -0.93$, lag $= 1$ month; Fig. 4e).

These correlations suggest that, when mode 1 is in positive phase, SST is warm in the Barents Sea, the subsurface AW temperature is warmer than average, sea ice extent is low, and SAT is warmer than average. A mechanism that could explain this mode is an increase in the temperature of the AW inflow to the Barents Sea, which would in turn reduce sea ice extent in the Barents Sea, both acting to increase AW heat loss to the atmosphere (Smedsrud et al. 2010) and resulting in warmer SAT. During a positive phase of this mode, both the increase of oceanic heat lost and the decrease of the sea ice extent will most likely affect the formation of BSW, as discussed in more detail in section 5.

We could not find a significant correlation between PC1 and SLP variations across the Barents Sea. This is at odds with the results of Herbaut et al. (2015), which suggested a link between the variations sea ice (and thus SST) and SLP. The different results could be due to the different periods considered as they only considered the variations up to 2004.

In summary, our lagged correlation analysis is consistent with heat carried in the AW inflow gradually influencing both SAT and BSW SST as it propagates

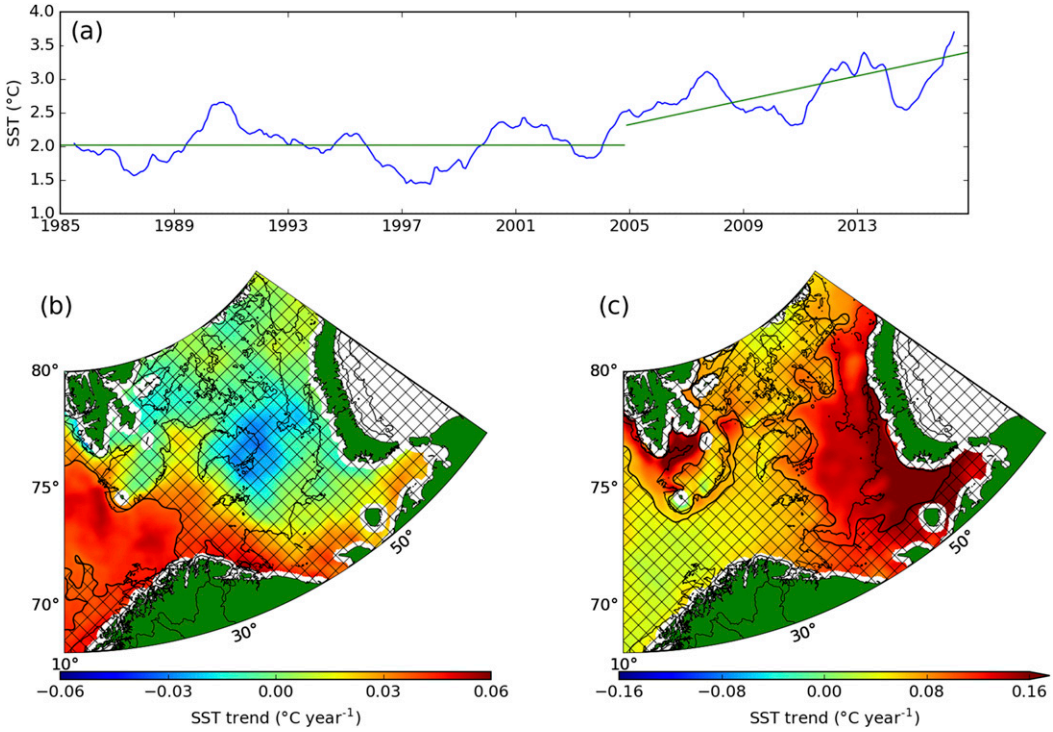

FIG. 5. (a) Mean SST across the Barents Sea with a 12-month running mean (blue line). The linear trend for the periods 1985–2004 and December 2004–16 are shown (green lines). Trend in SST for the periods (b) 1985–2004 and (c) 2005–16. Note that a different color scale is used in the two panels. Trends are significant at a level of 95% in unhatched areas. The black line indicates the 220-m isobath.

from Fugløya–Bear Island section to the Kola section and onward to the interior Barents Sea where SAT can feed heat back to SST. Our results suggest AW inflow temperature may be at least as important as SAT in setting the Barents Sea SST. Indeed, this BSW–SST forcing mechanism is supported by the conclusions of Smedsrud et al. (2010), who found that AW heat input has a bigger impact on SST variability than SAT forcing. The mechanism proposed here is also consistent with the results of Schlichtholz and Houssais (2011), who found that the temperature of recirculating AW exiting the Barents Sea through the BSO was driven by SAT within the Barents Sea.

We now examine the SST multidecadal variability. We find a significant positive linear trend of up to 0.05°C yr^{-1} in the western Barents Sea for the period from 1985 to 2004 (pre-2005; Fig. 5b). Post-2005 (2005–16), however, the SST in the western Barents Sea stabilizes, such that the trend becomes insignificant here while a positive trend of roughly 0.10°C yr^{-1} arises in most of the eastern Barents Sea (Fig. 5c). A positive trend is also found in the analysis of Singh et al. (2013) for the time period 2002–10. The shift in SST trend since 2005 is consistent with the results of Herbaut et al. (2015), who found a significant reduction of both the mean and variance of the winter sea ice concentration after 2005. The positive trend in the eastern Barents Sea coincides with an increase in AW temperatures observed at the Kola section (Fig. 4e). As AW temperature at the Kola section is correlated with PC1, it suggests mode 1 also captured part of the variability at multidecadal or longer time scales. As suggested by Smedsrud et al. (2010), an increase in AW heat transport would manifest in an expansion of a warm heat anomaly in the Barents Sea basin, resulting in an increase in the surface area in which heat loss takes place. The change in trend across the eastern Barents Sea could represent the expansion of this surface area.

Although the SST dataset is limited to 1985 onward, there are other datasets that have been used to address longer-term variability in the Barents Sea. A 16–20-yr and 30–50-yr time-scale fluctuation was found in ~100-yr observational datasets of both sea ice concentration and SLP (Venegas and Mysak 2000). These time scales are too long to be fully resolved in our analysis period, so we cannot fully distinguish between long-term trend and natural variations occurring on these time scales. Yet, the results of Venegas and Mysak (2000) suggest that the sea ice extent variations on the 16–20-yr time scale are

likely linked with SLP anomalies. Our time period of 32 years should capture some variability at the 16–20-yr time period that could be manifested as the change in temperature occurring in 2005. However, as our EOF1 is not driven by SLP variations, we hypothesize that the change occurring in 2005 is likely the manifestation of a regime shift rather than natural variability causing SLP to become decoupled across this time period. This hypothesis is also supported by the analysis of the observed sea ice extent from 1850 onward by Onarheim and Årthun (2017), who found that the winter sea ice extent has been consistently lower since 1990 than at any other time in the dataset. This is discussed in relation to long-term trends in section 5.

4. The PF's constraint on the sea ice edge

The magnitude of the 2D gradient in SST shows the surface manifestation of fronts in the Barents Sea (Figs. 2e–h). Starting in the west, a front follows Spitsbergen Bank but then bifurcates at Central Bank and splits into two branches (Fig. 2e), in agreement with the results of Oziel et al. (2016). The southern branch of this front (referred to hereafter as the Barents Sea Front) follows the western side of Central Bank southward, dividing the Barents Sea into an AW-influenced western region and a BSW-influenced eastern region. The Barents Sea Front is most prominent during winter and spring (Figs. 2e,h) and has been discussed in greater detail by Oziel et al. (2016, 2017).

Farther to the north, the PF divides the eastern Barents Sea into an ArW-influenced northern region and a BSW-influenced southern region. Our results show the PF to be a persistent feature following the ~220-m isobath throughout the year, although Oziel et al. (2016) found that the PF was positioned farther north than the present analysis with no fixed position. Their analysis was limited by the dataset used, comprising temperature and salinity in situ profiles collected in the Barents Sea, which captures only the subsurface expression of the front in the 50–100 m depth range. SST observations reveal that the PF pathway on the east side of the Barents Sea follows the southern sides of Great Bank and Ludlov Saddle eastward to Novaya Zemlya Bank (Figs. 2e–h). At Novaya Zemlya Bank, the PF extends northward along Novaya Zemlya Bank to 78°N. It should be noted that a second, weaker thermal-surface front exists in the SST data due to the transition from freezing ice-covered water to warmer ice-free water. The thermal-surface front does move with the sea ice edge and sometimes coincides with the more permanent PF.

Previous studies have investigated several aspects of the PF (Våge et al. 2014; Oziel et al. 2016), but the dynamics controlling it are still poorly pinned down. Here we present some evidences that the PF is controlled by potential vorticity constraints. Within the Barents Sea, the PF is closely tied to the 220-m isobath (Figs. 2, 3), which is located on a steep slope separating the northern and southern Barents Sea (Fig. 1). Potential vorticity constraints usually force currents to flow along topographic contours rather than across them (Taylor 1917; Proudman 1916). Planetary potential vorticity q can be estimated by the equation $q = f/h$, where f is the Coriolis parameter and h is the depth. The planetary potential vorticity contours in the Barents Sea follow closely the bathymetry contours as f is roughly constant in the region. In the case of a basin with a shallower northern outflow depth than inflow, that is, a ridge, an idealized model with potential vorticity constraints drives anticyclonic/clockwise circulation around the basin and eastward along the ridge in the Northern Hemisphere (Yang and Price 2000). This is consistent with the path of the PF we resolved by the OSTIA SST (Fig. 2), as well as the eastward flow found in velocity observations on the southwestern slope of Great Bank (Våge et al. 2014) and simulations showing eastward flow along the southern slope of Great Bank (Slagstad and McClimans 2005; Lind and Ingvaldsen 2012).

Following Pratt (2004), additional evidence that the PF is constrained by potential vorticity can be provided by estimating the Froude number associated with the flow across the ridge toward the eastern boundary (i.e., Novaya Zemlya Bank in our case). The Froude number is given by $F = u/(g'd)^{1/2}$, where u is current speed, g' is reduced gravity, and d is depth of the layer at the ridge. Here we take $u = 0.2\,\mathrm{m\,s^{-1}}$ (based on observations by Våge et al. (2014), assuming current speed is constant along the ridge), and values for g' and d are calculated from MIMOC data (see Fig. 7), obtaining a Froude number of 0.3. Following the argument developed by Pratt (2004) and given that in our case the height of the ridge occupies roughly one-third of the water column, a Froude number greater than 0.2 suggests that the Great Bank–Ludlov Saddle ridge imposes a hydraulic control on the flow associated with the PF, providing further evidence that the PF is constrained by potential vorticity.

We next examine time variations of the PF, in relation to the position of the sea ice edge over time. According to Smedsrud et al. (2010), the PF sets the limit on surface area available for winter heat loss over the Barents Sea. Logically, the PF may also play a role in determining the volume of summer freshwater input from sea ice meltwater. Thus, the interplay between the eastern Barents Sea PF and mobile sea ice edge mediates the properties of BSW that will be carried into the Arctic as AIW. A comparison of SST gradients and sea ice concentration

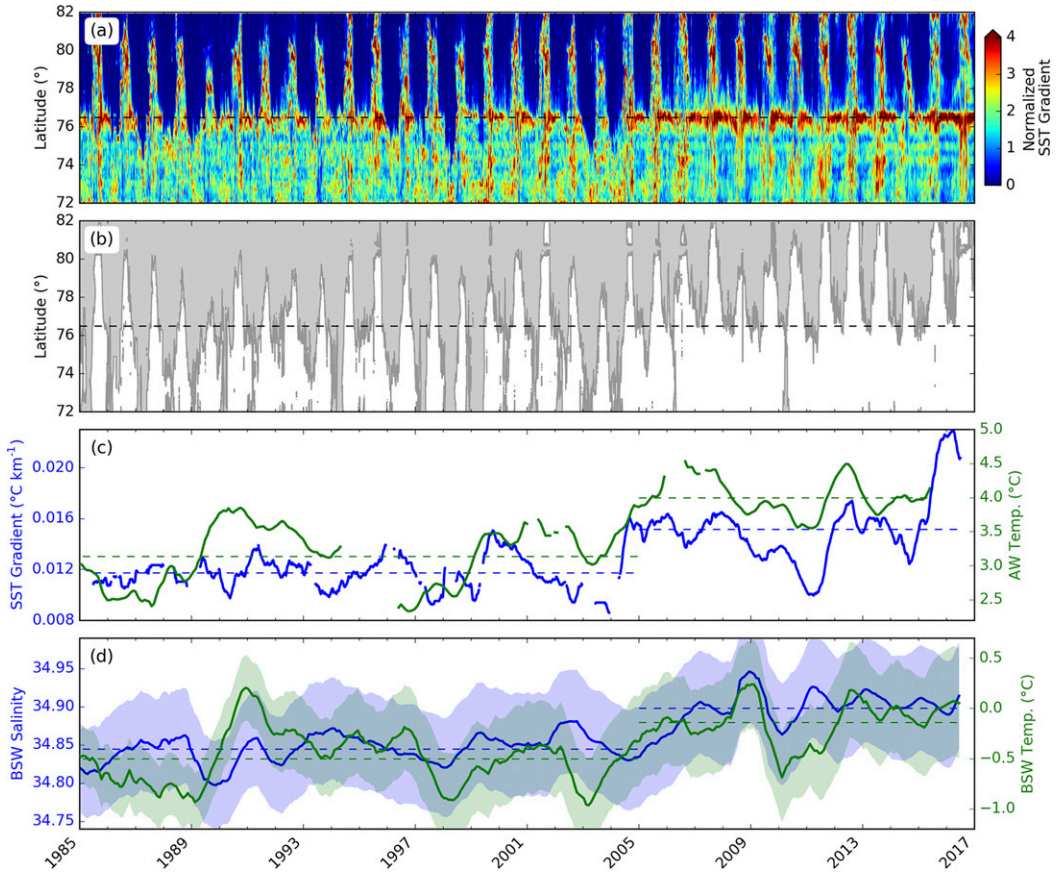

FIG. 6. (a) Magnitude of the meridional gradient in zonally averaged SST between 35° and 50°E (blue dashed box in Fig. 1) and PF location (dashed line). The magnitude is normalized on a daily basis by its standard deviation to show the changes in the position of the front over time. Note that changes in intensity over time cannot be deduced from (a). (b) Latitude of the sea ice edge for the same region. (c) Mean SST gradient between 76.3° and 76.7°N before normalization (blue line, 12-month running mean applied) and AW temperature from the Kola section (green line, 12-month running mean applied, section marked in Fig. 1). Gaps indicate missing data and sea ice coverage for AW and the SST gradient, respectively. (d) BSW salinity (blue line) and temperature (green line) between 100 and 300 m from the EN4 data, averaged in the cyan dashed box in Fig. 1. Uncertainty values for EN4 data are shown by the shaded areas. Dashed green and blue lines in (c) and (d) show the respective means for 1985–2004 and 2005–16.

shows that the sea ice edge follows the PF in both the eastern and western Barents Sea during winter and spring from 2005 to 2016 (Figs. 2a–d), but this was not the case before 2005 (Fig. 3). Steele and Ermold (2015) suggest that during the expansion and retreat of seasonal sea ice, the edge loiters at fronts where there is a gradient in temperature inhibiting further expansion. This then implies that the expansion of sea ice south of the PF before 2005 could be consistent with cooler SST or stronger northerly winds enabling greater transport of the mobile sea ice pack across the PF, enabling it to loiter closer to the Barents Sea Front.

We then focus on the interannual variability of the PF and its relationship with the sea ice edge (Fig. 6). To perform this analysis, the SST gradient is calculated meridionally and these gradients are averaged zonally within the box shown as a blue-dashed line in Fig. 1. Zonally averaged SST gradients on a given day are normalized by the daily standard deviation of the gradient in the same analysis box (Fig. 1), in order to remove the potential large effect of the strong seasonality and interannual variability in the intensity of the SST gradient. Figure 6a shows that the PF is persistent in its location throughout the majority of the year. Between 1985 and 2004, the PF was covered by sea ice for parts of winter and spring but held position at 76.5°N, rather than moving south with the advancing winter sea ice edge as previously thought (Smedsrud et al. 2010). As expected, there is also a thermal-surface front at the position of the sea ice edge to the north of the PF in

summer, but the PF is always present as a stronger and more persistent front at 76.5°N along the 220-m bathymetry contour.

A change in the location of the winter sea ice edge relative to the position of the PF is also evident on decadal time scales (Fig. 6). Unlike in the pre-2005 period, since 2005, the winter sea ice edge has been unable to sustain a southward breach of the PF for more than a few days (Fig. 6b). We define a region in the Barents Sea between the PF to the north and the Coastal Water front to the south shown by the dark-blue box in Fig. 1, within which sea ice melt can be entrained into BSW. The change in 2005 has reduced the mean seasonal change in sea ice area in this region, from 77 000 km^2 between 1985 and 2004 to 8700 km^2 between 2005 and 2016. This provides useful information in efforts to predict the location of the winter sea ice in the Barents Sea [examples of predictions include Onarheim and Årthun (2017), Sigmond et al. (2016), and Nakanowatari et al. (2014)]. This is important because changes in sea ice conditions in the Barents Sea have been linked to widespread, anomalous atmospheric conditions over northern continents (Petoukhov and Semenov 2010; Yang et al. 2016).

At the same time, while remaining fixed to topography, the mean SST gradient across the PF increases significantly from $0.011° \pm 10^{-4}$°C km^{-1} pre-2005 to $0.015° \pm 10^{-4}$°C km^{-1} post-2005 (Fig. 6c). This steepening in the PF SST gradient coincides with a significant increase in AW temperature at the Kola section from 3.1° ± 0.05°C in the pre-2005 period to 4.0° ± 0.05°C in the post-2005 period. Given that the SST north of the PF is changing at a slower rate than south of the PF (Fig. 5), the intensification of the PF can then be mainly attributed to the increase in AW temperature in the Barents Sea. One important consequence of the increase in AW temperature is that the heat content on the southern side of the front prevents sea ice from accumulating. A link between changes in sea ice and AW temperature has been discussed by Smedsrud et al. (2013) but not in relation to the PF. We assess this result in relation to trend and long-term variability in section 5.

In addition to the changes found in the southern side of the front, discussed above, changes in the properties of the ArW north of the PF could also occur. To the northeast of Svalbard where the AW lies close to the surface, Ivanov et al. (2016) have suggested that a positive feedback could exist between entrainment of warm AW and reduced midwinter sea ice thickness, due to a decrease of the stratification driven by change in salinity. The mean ArW properties from EN4 pre-2005 were $T = -1.15° \pm 0.04$°C, $S = 34.463 \pm 0.014$, while post-2005 they were $T = -0.76° \pm 0.06$°C, $S = 34.569 \pm 0.022$ (Fig. 1 shows the cyan dashed box selected for ArW properties north of the PF). This significant increase in temperature and salinity could be caused by a similar process to the one described by Ivanov et al. (2016).

The mean surface BSW properties pre-2005 were $T = -0.22° \pm 0.03$°C, $S = 34.828 \pm 0.009$, while post-2005 they significantly increased to $T = 0.50° \pm 0.05$°C, $S = 34.943 \pm 0.013$ (Fig. 1 shows the yellow dashed box selected for surface BSW properties south of the PF). The salinity increase is comparable for the surface BSW and ArW within the error bounds, but the increase in the temperature of surface BSW is almost double the change in ArW temperature over the same period. The result on ArW density and surface BSW density is an increase of 0.071 ± 0.017 kg m^{-3} and 0.054 ± 0.009 kg m^{-3}, respectively, indicating a decrease in the density gradient across the PF after 2005. This suggests that the steepening of the temperature gradient and weakening of the density gradient across the PF in the eastern Barents Sea are primarily driven by changes occurring in the southern side of the PF.

Transect data through the eastern Barents Sea (Fig. 7) show the SST gradient across the PF is the surface expression of a vertically coherent front. In both the EN4 and MIMOC climatologies, the PF is present near 76.5°N as a negative south–north temperature gradient over the depth range 0–100 m, and a similar subsurface salinity gradient. The PF is a transition between the southern region that is temperature-stratified (α ocean) and the northern region that is salinity-stratified (β ocean; Carmack 2007). Here, α is the coefficient of thermal expansion, and β is the coefficient of haline contraction. This makes the PF an important transition zone where the contribution to density from temperature and salinity can be in balance. Note the presence of water that is too fresh to fit the BSW definition and too warm to fit the ArW definition between 77° and 78°N over 0–50 m (Figs. 7b,d). This water mass sits on the mixing line between BSW and ArW (Fig. 7h), suggesting that mixing between BSW and ArW occurs at the front. Previous studies based on observations in the western Barents Sea have revealed the presence of interleaving between BSW and ArW along the PF that could enhance mixing (Parsons et al. 1996; Våge et al. 2014; Fer and Drinkwater 2014).

On the northern side of the transect, the ArW layer (Table 1) is present in the MIMOC data over the depth range 0–100 m at 80°N and extends down to 50 m at 77°N. In EN4, the ArW layer extends to a deeper depth of 150 m at 80°N and 100 m at 77°N. The main difference between the EN4 climatology and the MIMOC climatology is the 1°C cooler temperature of BSW in the EN4 than in MIMOC (Figs. 7c,d). This may represent a change in BSW temperature over time given that the MIMOC climatology is weighted to be characteristic

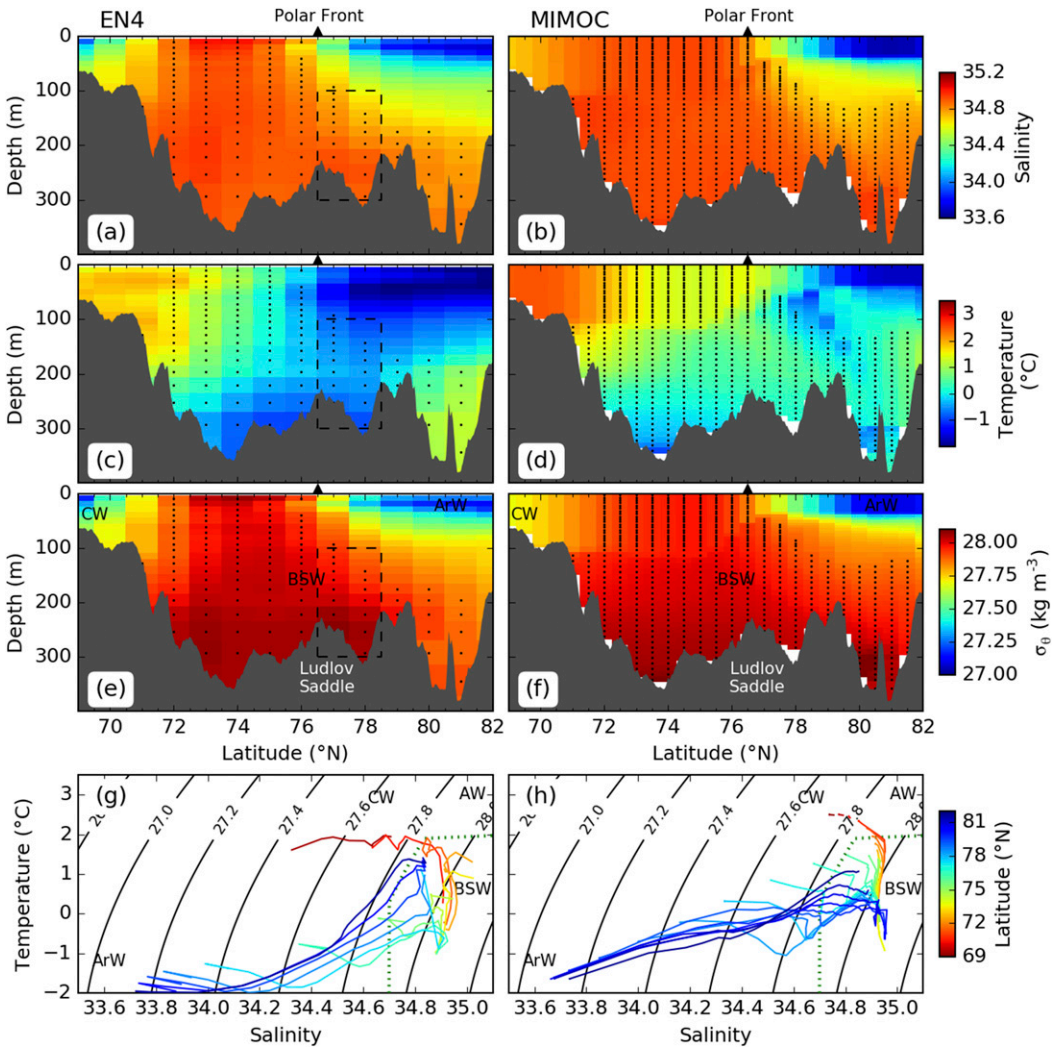

FIG. 7. Eastern Barents Sea transect at 44°E (shown in Fig. 1) from the MIMOC and EN4 climatology during winter (December–February); EN4 is averaged over 1985–2016. The PF is marked by the black triangle. (a),(b) Salinity; (c),(d) temperature; and (e),(f) potential density. White areas in (a)–(f) indicate grid cells with no data, black points show the grid cells containing BSW, and the black dashed areas indicate the EN4 subsection used to produce the BSW temperature and salinities (Fig. 6). (g),(h) Temperature–salinity diagrams showing the different water masses present in (a)–(f). The color indicates the latitude of the profile. The green dotted area in (g) and (h) shows the limits of the BSW definitions, and AW, ArW, and CW water masses are indicated (see Table 1 for their definitions).

of 2007–11 whereas the EN4 climatology is an average over the period 1985–2016. Regardless of the difference in temperature between the two datasets, BSW occupies roughly the same area (black dots in Figs. 7e,f). As BSW is denser than ArW (Figs. 7g,h), it sits below ArW north of the PF at 76.5°N. From Ludlov Saddle, BSW flows eastward and exits the Barents Sea through St. Anna Trough in a layer below ArW (Schauer et al. 2002). As the Central basin is the source of BSW (Oziel et al. 2016), this suggests BSW propagates northward of the PF either by subducting below ArW or by undergoing modification at the surface due to fast-mixing processes in the upper portion of BSW that Rudels et al. (1996) has hypothesized occurs during winter heat loss.

5. Atlantification of the Barents Sea and implications for Barents Sea Water

As a consequence of the intensification of the PF since 2005, it now forms a persistent barrier to the formation and export of sea ice south of the PF (Fig. 6). Having identified the forcing on BSW in section 3, here we discuss the possible implications of the barrier imposed by the PF on the properties of the BSW exiting the Barents Sea:

1) The northern limit of the surface area available for AW winter heat loss has become fixed to the location of the PF. The subsurface EN4-averaged BSW temperature has warmed from $-0.51° \pm 0.03°C$ to $-0.13° \pm 0.03°C$ when comparing the pre-2005 and post-2005 periods (Fig. 6c, averaged over 100–300 m in the cyan dashed box in Fig. 1). The increase of the temperature at the Kola section between the same two periods is more than twice as large (0.9°C). The observed reduction in Barents Sea ice extent has resulted in an increase of the surface heat flux from the ocean to the atmosphere (Long and Perrie 2017; Årthun et al. 2012), likely explaining the different rate of temperature increase between the BSW and the Kola section.

   Before 2005, the expansion and retreat of sea ice in the eastern Barents Sea buffered BSW properties against changes in AW temperatures (Smedsrud et al. 2010), but our analysis suggests that this buffering capacity has reduced since 2005, enabling the temperature increase of BSW in recent years visible in Fig. 6d. Such a temperature change requires that most of the AW heat is lost to the atmosphere in the ice-free southern Barents Sea [which is consistent with the results of Smedsrud et al. (2010)] and that the heat lost by BSW through mixing with ArW north of the PF is small. While Lind et al. (2016) have pointed out that mixing between ArW and BSW can exist, in particular during years with lower sea ice cover, the heat lost through that process is most likely much smaller than the heat lost to the atmosphere south of the PF.
2) The reduction of sea ice south of the PF reduces the seasonal freshwater input to BSW associated with local sea ice melt. Based on their model simulations, Ellingsen et al. (2009) found that between 1979 and 2007, meltwater from imported sea ice contributed 0.02 Sv ($1\,\text{Sv} \equiv 10^6\,\text{m}^3\,\text{s}^{-1}$) of freshwater on average. This is enough to decrease the mean salinity of their simulated 1.1 Sv AW inflow (salinity 35.1) to salinity of 34.4. However, in their study, Ellingsen et al. (2009) does not account for the PF's role in partitioning sea ice meltwater between BSW and ArW and considers that the input of sea ice meltwater takes place entirely south of the PF, and thus can convert AW into ArW. Here we revisit their calculation, taking into account the partitioning of meltwater at the PF.

   To calculate the meltwater input south of the PF before 2005, we assume that the sea ice found south of the front was 1 m thick, which is a typical thickness for first-year ice in the Barents Sea (Ellingsen et al. 2009; Smedsrud et al. 2010). In contrast to Ellingsen et al. (2009), we only consider the box that contains the area south of the PF and north of the Coastal Water front shown by the dark-blue box in Fig. 1, and assume that the AW is not modified before it enters that box. Within this box, the reduction in sea ice area south of the PF by 68 300 km^2 between the pre and post-2005 periods (Fig. 6) corresponds to a 0.0022-Sv reduction in the freshwater input south of the PF after 2005 when the sea ice is no longer present. This is assumed to mix ubiquitously into BSW.

   To calculate the dilution of AW by sea ice melt, we estimate the volume to be diluted by comparing the AW inflow to the BSW outflow. Following Gammelsrød et al. (2009), we assume a BSW transport leaving the Barents Sea between Novaya Zemlya and Franz-Josef Land of 1.25 Sv (observed transport scaled up by the difference between virtual current meters and modeled, whole-section transport). For comparison the net annual observed AW inflow through the BSO is 1.1–1.2 Sv (excluding transport associated with Norwegian Coastal Current; Skagseth 2008; Ingvaldsen et al. 2004). This implies that there is no net storage of BSW in the Barents Sea, such that the volume of AW to be diluted is $V_{\text{AW}} = 1.1$ Sv (note, a change of AW volume transport across our time period cannot be estimated from the available observations).

   The salinity of inflowing AW should also be taken into account when calculating a change in BSW salinity. As shown in Fig. 4d, the mean properties of AW at the Fugløya–Bear Island section for 1985–2005 were $T = 5.44° \pm 0.06°C$, $S = 35.067 \pm 0.003$, and for 2005–2016 they were $T = 6.08° \pm 0.07°C$, $S = 35.120 \pm 0.005$ (the changes between the two periods are significant). Using these different salinity values and considering that the input of freshwater south of the PF vanishes after 2005, we perform a simple dilution calculation, following the equation $C = (M_{\text{AW}} + M_{\text{FW}})/(V_{\text{AW}} + V_{\text{FW}})$, where C is the concentration of salt, M is the mass of salt, V is the volume, AW is Atlantic Water, and FW is fresh sea ice meltwater. We also assume a constant salinity value of 3 for first-year sea ice (Ellingsen et al. 2009) and constant net AW inflow (BSW outflow) of 1.1 Sv (1.25 Sv) (Skagseth 2008; Gammelsrød et al. 2009). Based on this framework, pre-2005 the mean input of 0.0022 Sv of freshwater results in a freshening of -0.063 (-0.056) of the BSW salinity, while post-2005, the BSW salinity would equal the AW salinity which additionally became more saline by 0.053 across this time period. Our dilution calculation predicts a change of BSW salinity by ~0.11, which is in broad agreement with the significant increase of BSW salinity estimated from the EN4 dataset (from 34.844 ± 0.003 to 34.900 ± 0.002; Fig. 6c). This

suggests that the increase in BSW salinity is likely a combination of the change in sea ice area and the change in inflowing AW salinity.

When comparing the mean BSW temperature over the two periods in EN4, it increases by 0.38°C, which is about a half of the 0.8°C required to compensate density changes arising from the 0.056 mean salinity increase observed. These changes in temperature and salinity have led to a significant increase of BSW density from 1029.092 ± 0.002 kg m^{-3} pre-2005 to 1029.116 ± 0.002 kg m^{-3} post-2005.

The 0.024 kg m^{-3} increase in BSW density between the two periods has to be compared against the gain in density resulting from the transformation of AW to BSW. Pre-2005, the density transformation amounted to ~0.33 kg m^{-3}, a combination of 5.9°C decrease and 0.23 salinity decrease (based on AW properties at the BSO). This means a further 8% density change in BSW relative to the pre-2005 era.

Our comparison of the two periods (pre- and post-2005) suggests that a regime shift occurred in 2005. Yet, one needs to remember that there is well-known multidecadal variability affecting SLP, sea ice concentration, SAT, and AW temperature (Venegas and Mysak 2000; Smedsrud et al. 2013; Levitus et al. 2009; Ingvaldsen et al. 2003). Variability at a 30–50-yr frequency is thought to be driven by the Atlantic multidecadal oscillation, suggesting that long-term variations in the Barents Sea are driven by large-scale fluctuations (Levitus et al. 2009). These variations are also affecting the formation, properties, and volume of BSW on similar time scales (Årthun et al. 2011). Analysis by Onarheim and Årthun (2017) of an observed time series of winter sea ice extent from 1850 to 2017 in the Barents Sea complemented by analysis of climate simulations also emphasizes the existence of variations with a 50-yr periodicity. However, their results show winter sea ice extent in the Barents Sea has been lower since 1990 than in the rest of the time period and that there is an unprecedented negative trend in the last 30 years that has less than 5% probability of occurring in all preindustrial simulations. This suggests that winter sea ice in the Barents Sea has most likely not been inhibited by the PF during 1850–2005. Further evidence comes from the observations by Smedsrud et al. (2013), suggesting that Arctic SAT and AW temperature at the Kola section were both greater after ~2000 than at any time from the last century.

6. Conclusions

The goal of this study was to investigate how changes and feedbacks between sea ice and the PF in the Barents Sea may have affected BSW properties over the past decades. We have identified and located the PF in the eastern Barents Sea using satellite SST observations, a feature that has been obscured by seasonal sea ice between 1985 and 2004. While a summer mixed layer and seasonal front does form in association with the melt of seasonal sea ice, as is the case in other regions (Dewey et al. 2017), the PF persists throughout the year as a front with steeper gradients in salinity and temperature in the eastern Barents Sea at 76.5°N, running parallel to the 220-m isobath (Fig. 2). The PF is a potential-vorticity-constrained, shelf slope current at the steep ridge formed by Great Bank and Ludlov Saddle. Since 2005, the sea ice is inhibited in its winter southward extent by the increase in temperature gradients across the PF, a change most likely driven by an increase in AW temperature.

Our results provide new evidence that, in addition to the natural multidecadal variability, the Barents Sea is currently undergoing Atlantification, with the corresponding temperature and salinity increases catalyzed by the observed PF constraint on the sea ice edge. The loss of winter sea ice south of the front represents a loss of freshwater input to BSW, a water mass that makes up 50%–80% of AIW. As the stationary PF, rather than the mobile sea ice edge, has become the limiting factor controlling the northern boundary of the surface area available for AW cooling in winter, the buffering effect to BSW temperature from the variations of sea ice conditions has decreased. Observations show a change in BSW properties over the same time period resulting in denser BSW, which could in turn result in a deeper settling depth of BSW once exported to the Arctic basin through St. Anna Trough (Dmitrenko et al. 2015), with potential far-reaching impacts for the dense water outflow through Fram Strait (Lique et al. 2010; Moat et al. 2014) or the density of the Denmark Strait overflow (Karcher et al. 2011), both of which are important for the deeper branch of the AMOC.

Acknowledgments. This project was funded through the joint U.K.–France PhD program by DGA/Dstl, and overseen by Carole Nahum and Timothy Clarke. Data from the Fugløya–Bear Island section are provided courtesy of Institute of Marine Research, Norway.

REFERENCES

Aagaard, K., and R. A. Woodgate, 2001: Some thoughts on the freezing and melting of sea ice and their effects on the ocean. *Ocean Modell.*, **3**, 127–135, https://doi.org/10.1016/S1463-5003(01)00005-1.

——, J. H. Swift, and E. C. Carmack, 1985: Thermohaline circulation in the Arctic Mediterranean Seas. *J. Geophys. Res.*, **90**, 4833–4846, https://doi.org/10.1029/JC090iC03p04833.

Årthun, M., R. B. Ingvaldsen, L. H. Smedsrud, and C. Schrum, 2011: Dense water formation and circulation in the Barents Sea. *Deep-Sea Res. I*, **58**, 801–817, https://doi.org/10.1016/j.dsr.2011.06.001.

——, T. Eldevik, L. H. Smedsrud, Ø. Skagseth, and R. B. Ingvaldsen, 2012: Quantifying the influence of Atlantic heat on Barents sea ice variability and retreat. *J. Climate*, **25**, 4736–4743, https://doi.org/10.1175/JCLI-D-11-00466.1.

Berrisford, P., and Coauthors, 2011: The ERA-Interim Archive: Version 2.0. ERA Rep. Series 1, 23 pp., https://www.ecmwf.int/sites/default/files/elibrary/2011/8174-era-interim-archive-version-20.pdf.

Bochkov, Y. A., 1982: Water temperature in the 0-200 m layer in the Kola-Meridian section in the Barents Sea, 1900–1981 (in Russian). *Sb. Nauchn. Tr. PINRO Murm.*, **46**, 113–122.

Carmack, E. C., 2007: The alpha/beta ocean distinction: A perspective on freshwater fluxes, convection, nutrients and productivity in high-latitude seas. *Deep-Sea Res. II*, **54**, 2578–2598, https://doi.org/10.1016/j.dsr2.2007.08.018.

Day, J. J., S. Tietsche, and E. Hawkins, 2014: Pan-arctic and regional sea ice predictability: Initialization month dependence. *J. Climate*, **27**, 4371–4390, https://doi.org/10.1175/JCLI-D-13-00614.1.

Dewey, S. R., J. H. Morison, and J. Zhang, 2017: An edge-referenced surface fresh layer in the Beaufort Sea seasonal ice zone. *J. Phys. Oceanogr.*, **47**, 1125–1144, https://doi.org/10.1175/JPO-D-16-0158.1.

Ding, Y., J. A. Carton, G. A. Chepurin, M. Steele, and S. Hakkinen, 2016: Seasonal heat and freshwater cycles in the Arctic Ocean in CMIP5 coupled models. *J. Geophys. Res. Oceans*, **121**, 2043–2057, https://doi.org/10.1002/2015JC011124.

Dmitrenko, I. A., and Coauthors, 2014: Heat loss from the Atlantic water layer in the northern Kara Sea: Causes and consequences. *Ocean Sci.*, **10**, 719–730, https://doi.org/10.5194/os-10-719-2014.

——, and Coauthors, 2015: Atlantic water flow into the Arctic Ocean through the St. Anna Trough in the northern Kara Sea. *J. Geophys. Res. Oceans*, **120**, 5158–5178, https://doi.org/10.1002/2015JC010804.

Donlon, C. J., M. Martin, J. Stark, J. Roberts-Jones, E. Fiedler, and W. Wimmer, 2012: The Operational Sea Surface Temperature and Sea Ice Analysis (OSTIA) system. *Remote Sens. Environ.*, **116**, 140–158, https://doi.org/10.1016/j.rse.2010.10.017.

Ellingsen, I., D. Slagstad, and A. Sundfjord, 2009: Modification of water masses in the Barents Sea and its coupling to ice dynamics: A model study. *Ocean Dyn.*, **59**, 1095–1108, https://doi.org/10.1007/s10236-009-0230-5.

Fahrbach, E., J. Meincke, S. Österhus, G. Rohardt, U. Schauer, V. Tverberg, J. Verduin, and R. A. Woodgate, 2001: Direct measurements of heat and mass transports through the Fram Strait. *Polar Res.*, **20**, 217–224, https://doi.org/10.3402/polar.v20i2.6520.

Fer, I., and K. Drinkwater, 2014: Mixing in the Barents Sea Polar Front near Hopen in spring. *J. Mar. Syst.*, **130**, 206–218, https://doi.org/10.1016/j.jmarsys.2012.01.005.

Gammelsrød, T., Ø. Leikvin, V. Lien, W. P. Budgell, H. Loeng, and W. Maslowski, 2009: Mass and heat transports in the NE Barents Sea: Observations and models. *J. Mar. Syst.*, **75**, 56–69, https://doi.org/10.1016/j.jmarsys.2008.07.010.

Gawarkiewicz, G., and A. J. Plueddemann, 1995: Topographic control of thermohaline frontal structure in the Barents Sea Polar Front on the south flank of Spitsbergen Bank. *J. Geophys. Res.*, **100**, 4509–4524, https://doi.org/10.1029/94JC02427.

Good, S. A., M. J. Martin, and N. A. Rayner, 2013: EN4: Quality controlled ocean temperature and salinity profiles and monthly objective analyses with uncertainty estimates. *J. Geophys. Res. Oceans*, **118**, 6704–6716, https://doi.org/10.1002/2013JC009067.

Gouretski, V., and F. Reseghetti, 2010: On depth and temperature biases in bathythermograph data: Development of a new correction scheme based on analysis of a global ocean database. *Deep-Sea Res. I*, **57**, 812–833, https://doi.org/10.1016/j.dsr.2010.03.011.

Harris, C. L., A. J. Plueddemann, and G. G. Gawarkiewicz, 1998: Water mass distribution and polar front structure in the western Barents Sea. *J. Geophys. Res.*, **103**, 2905–2917, https://doi.org/10.1029/97JC02790.

Herbaut, C., M.-N. Houssais, S. Close, and A.-C. Blaizot, 2015: Two wind-driven modes of winter sea ice variability in the Barents Sea. *Deep-Sea Res. I*, **106**, 97–115, https://doi.org/10.1016/j.dsr.2015.10.005.

Ingvaldsen, R. B., 2005: Width of the North Cape Current and location of the Polar Front in the western Barents Sea. *Geophys. Res. Lett.*, **32**, L16603, https://doi.org/10.1029/2005GL023440.

——, H. Loeng, O. Geir, and A. Bjorn, 2003: Climate variability in the Barents Sea during the 20th century with a focus on the 1990s. *ICES Mar. Sci. Symp.*, **219**, 160–168, http://www.ices.dk/sites/pub/PublicationReports/MarineScienceSymposia/Phase2/ICESMarineScienceSymposia-Volume219-2003-Part20of75.pdf.

——, L. Asplin, and H. Loeng, 2004: The seasonal cycle in the Atlantic transport to the Barents Sea during the years 1997–2001. *Cont. Shelf Res.*, **24**, 1015–1032, https://doi.org/10.1016/j.csr.2004.02.011.

Ivanov, V., V. Alexeev, N. V. Koldunov, I. Repina, A. B. Sandø, L. H. Smedsrud, and A. Smirnov, 2016: Arctic Ocean heat impact on regional ice decay: A suggested positive feedback. *J. Phys. Oceanogr.*, **46**, 1437–1456, https://doi.org/10.1175/JPO-D-15-0144.1.

Karcher, M., A. Beszczynska-Möller, F. Kauker, R. Gerdes, S. Heyen, B. Rudels, and U. Schauer, 2011: Arctic Ocean warming and its consequences for the Denmark Strait overflow. *J. Geophys. Res.*, **116**, C02037, https://doi.org/10.1029/2010JC006265.

Koenigk, T., U. Mikolajewicz, J. H. Jungclaus, and A. Kroll, 2009: Sea ice in the Barents Sea: Seasonal to interannual variability and climate feedbacks in a global coupled model. *Climate Dyn.*, **32**, 1119–1138, https://doi.org/10.1007/s00382-008-0450-2.

Kwok, R., 2009: Outflow of Arctic Ocean sea ice into the Greenland and Barents Seas: 1979–2007. *J. Climate*, **22**, 2438–2457, https://doi.org/10.1175/2008JCLI2819.1.

Larsen, K. M. H., C. Gonzalez-Pola, P. Fratantoni, A. Beszczynska-Möller, and S. L. E. Hughes, 2016: ICES Report on Ocean Climate 2015. ICES Cooperative Research Rep. 331, 79 pp., http://www.ices.dk/sites/pub/Publication%20Reports/Cooperative%20Research%20Report%20(CRR)/crr331/CRR%20331.pdf.

Levitus, S., G. Matishov, D. Seidov, and I. Smolyar, 2009: Barents Sea multidecadal variability. *Geophys. Res. Lett.*, **36**, L19604, https://doi.org/10.1029/2009GL039847.

Lien, V. S., P. Schlichtholz, Ø. Skagseth, and F. B. Vikebø, 2017: Wind-driven Atlantic water flow as a direct mode for reduced Barents Sea ice cover. *J. Climate*, **30**, 803–812, https://doi.org/10.1175/JCLI-D-16-0025.1.

Lind, S., and R. B. Ingvaldsen, 2012: Variability and impacts of Atlantic Water entering the Barents Sea from the north. *Deep-Sea Res. I*, **62**, 70–88, https://doi.org/10.1016/j.dsr.2011.12.007.

——, ——, and T. Furevik, 2016: Arctic layer salinity controls heat loss from deep Atlantic layer in seasonally ice-covered areas of the Barents Sea. *Geophys. Res. Lett.*, **43**, 5233–5242, https://doi.org/10.1002/2016GL068421.

Lique, C., A. M. Treguier, B. Blanke, and N. Grima, 2010: On the origins of water masses exported along both sides of Greenland:

A Lagrangian model analysis. *J. Geophys. Res. Oceans*, **115**, C05019, https://doi.org/10.1029/2009JC005316.

Loeng, H., 1991: Features of the physical oceanographic conditions of the Barents Sea. *Polar Res.*, **10**, 5–18, https://doi.org/10.3402/polar.v10i1.6723.

Long, Z., and W. Perrie, 2017: Changes in ocean temperature in the Barents Sea in the twenty-first century. *J. Climate*, **30**, 5901–5921, https://doi.org/10.1175/JCLI-D-16-0415.1.

Maslowski, W., D. Marble, W. Walczowski, U. Schauer, J. L. Clement, and A. J. Semtner, 2004: On climatological mass, heat, and salt transports through the Barents Sea and Fram Strait from a pan-Arctic coupled ice-ocean model simulation. *J. Geophys. Res.*, **109**, C03032, https://doi.org/10.1029/2001JC001039.

McDougall, T. J., D. R. Jackett, F. J. Millero, R. Pawlowicz, and P. M. Barker, 2012: A global algorithm for estimating Absolute Salinity. *Ocean Sci.*, **8**, 1123–1134, https://doi.org/10.5194/os-8-1123-2012.

Moat, B., S. Josey, and B. Sinhu, 2014: Impact of Barents Sea winter air-sea exchanges on Fram Strait dense water transport. *J. Geophys. Res. Oceans*, **119**, 1009–1021, https://doi.org/10.1002/2013JC009220.

Nakanowatari, T., K. Sato, and J. Inoue, 2014: Predictability of the Barents Sea ice in early winter: Remote effects of oceanic and atmospheric thermal conditions from the North Atlantic. *J. Climate*, **27**, 8884–8901, https://doi.org/10.1175/JCLI-D-14-00125.1.

Notz, D., and J. Stroeve, 2016: Observed Arctic sea-ice loss directly follows anthropogenic CO_2 emission. *Science*, **354**, 747–750, https://doi.org/10.1126/science.aag2345.

Onarheim, I. H., and M. Årthun, 2017: Toward an ice-free Barents Sea. *Geophys. Res. Lett.*, **44**, 8387–8395, https://doi.org/10.1002/2017GL074304.

——, T. Eldevik, M. Årthun, R. B. Ingvaldsen, and L. H. Smedsrud, 2015: Skillful prediction of Barents Sea ice cover. *Geophys. Res. Lett.*, **42**, 5364–5371, https://doi.org/10.1002/2015GL064359.

Oziel, L., J. Sirven, and J. C. Gascard, 2016: The Barents Sea frontal zones and water masses variability (1980–2011). *Ocean Sci.*, **12**, 169–184, https://doi.org/10.5194/os-12-169-2016.

——, and Coauthors, 2017: Role for Atlantic inflows and sea ice loss on shifting phytoplankton blooms in the Barents Sea. *J. Geophys. Res. Oceans*, **122**, 5121–5139, https://doi.org/10.1002/2016JC012582.

Parsons, A. R., R. H. Bourke, R. D. Muench, C.-S. Chiu, J. F. Lynch, J. H. Miller, A. J. Plueddemann, and R. Pawlowicz, 1996: The Barents Sea Polar Front in summer. *J. Geophys. Res.*, **101**, 14 201–14 221, https://doi.org/10.1029/96JC00119.

Petoukhov, V., and V. A. Semenov, 2010: A link between reduced Barents-Kara sea ice and cold winter extremes over northern continents. *J. Geophys. Res.*, **115**, D21111, https://doi.org/10.1029/2009JD013568.

Polyakov, I. V., and Coauthors, 2017: Greater role for Atlantic inflows on sea-ice loss in the Eurasian Basin of the Arctic Ocean. *Science*, **356**, 285–291, https://doi.org/10.1126/science.aai8204.

Pratt, L. J., 2004: Recent progress on understanding the effects of rotation in models of sea straits. *Deep-Sea Res. II*, **51**, 351–369, https://doi.org/10.1016/j.dsr2.2003.06.005.

Proudman, J., 1916: On the motion of solids in a liquid possessing vorticity. *Proc. Roy. Soc. London*, **92A**, 408–424, https://doi.org/10.1098/rspa.1916.0026.

Reigstad, M., P. Wassmann, C. Wexels Riser, S. Øygarden, and F. Rey, 2002: Variations in hydrography, nutrients and chlorophyll a in the marginal ice-zone and the central Barents Sea. *J. Mar. Syst.*, **38**, 9–29, https://doi.org/10.1016/S0924-7963(02)00167-7.

Rudels, B., L. G. Anderson, and E. P. Jones, 1996: Formation and evolution of the surface mixed layer and halocline of the Arctic Ocean. *J. Geophys. Res.*, **101**, 8807–8821, https://doi.org/10.1029/96JC00143.

——, R. D. Muench, J. Gunn, U. Schauer, and H. J. Friedrich, 2000: Evolution of the Arctic Ocean boundary current north of the Siberian shelves. *J. Mar. Syst.*, **25**, 77–99, https://doi.org/10.1016/S0924-7963(00)00009-9.

——, M. Korhonen, U. Schauer, S. Pisarev, B. Rabe, and A. Wisotzki, 2015: Circulation and transformation of Atlantic water in the Eurasian Basin and the contribution of the Fram Strait inflow branch to the Arctic Ocean heat budget. *Prog. Oceanogr.*, **132**, 128–152, https://doi.org/10.1016/j.pocean.2014.04.003.

Schauer, U., R. D. Muench, B. Rudels, and L. Timokhov, 1997: Impact of eastern Arctic shelf waters on the Nansen Basin intermediate layers. *J. Geophys. Res.*, **102**, 3371–3382, https://doi.org/10.1029/96JC03366.

——, H. Loeng, B. Rudels, V. K. Ozhigin, and W. Dieck, 2002: Atlantic Water flow through the Barents and Kara Seas. *Deep-Sea Res. I*, **49**, 2281–2298, https://doi.org/10.1016/S0967-0637(02)00125-5.

Schlichtholz, P., and M. N. Houssais, 2011: Forcing of oceanic heat anomalies by air-sea interactions in the Nordic Seas area. *J. Geophys. Res.*, **116**, C01006, https://doi.org/10.1029/2009JC005944.

Schmidtko, S., G. C. Johnson, and J. M. Lyman, 2013: MIMOC: A global monthly isopycnal upper-ocean climatology with mixed layers. *J. Geophys. Res. Oceans*, **118**, 1658–1672, https://doi.org/10.1002/jgrc.20122.

Screen, J. A., and I. Simmonds, 2010: The central role of diminishing sea ice in recent Arctic temperature amplification. *Nature*, **464**, 1334–1337, https://doi.org/10.1038/nature09051.

Shapiro, G. I., 2003: Dense water cascading off the continental shelf. *J. Geophys. Res.*, **108**, 3390, https://doi.org/10.1029/2002JC001610.

Sigmond, M., M. C. Reader, G. M. Flato, W. J. Merryfield, and A. Tivy, 2016: Skillful seasonal forecasts of Arctic sea ice retreat and advance dates in a dynamical forecast system. *Geophys. Res. Lett.*, **43**, 12 457–12 465, https://doi.org/10.1002/2016GL071396.

Singh, R. K., M. Maheshwari, S. R. Oza, and R. Kumar, 2013: Long-term variability in Arctic sea surface temperatures. *Polar Sci.*, **7**, 233–240, https://doi.org/10.1016/j.polar.2013.10.003.

Skagseth, Ø., 2008: Recirculation of Atlantic Water in the western Barents Sea. *Geophys. Res. Lett.*, **35**, L11606, https://doi.org/10.1029/2008GL033785.

Slagstad, D., and T. A. McClimans, 2005: Modeling the ecosystem dynamics of the Barents Sea including the marginal ice zone: I. Physical and chemical oceanography. *J. Mar. Syst.*, **58**, 1–18, https://doi.org/10.1016/j.jmarsys.2005.05.005.

Smedsrud, L. H., R. Ingvaldsen, J. E. Ø. Nilsen, and Ø. Skagseth, 2010: Heat in the Barents Sea: Transport, storage, and surface fluxes. *Ocean Sci.*, **6**, 219–234, https://doi.org/10.5194/os-6-219-2010.

——, and Coauthors, 2013: The role of the Barents Sea in the Arctic climate system. *Rev. Geophys.*, **51**, 415–449, https://doi.org/10.1002/rog.20017.

Snape, T., 2013: Decline of Arctic Sea Ice: Evaluation and weighting of CMIP5 projections. *J. Geophys. Res. Atmos.*, **119**, 546–554, https://doi.org/10.1002/2013JD020593.

Sorteberg, A., and B. Kvingedal, 2006: Atmospheric forcing on the Barents Sea winter ice extent. *J. Climate*, **19**, 4772–4784, https://doi.org/10.1175/JCLI3885.1.

Steele, M., and W. Ermold, 2015: Loitering of the retreating sea ice edge in the Arctic Seas. *J. Geophys. Res. Oceans*, **120**, 7699–7721, https://doi.org/10.1002/2015JC011182.

Taylor, G. I., 1917: Motion of solids in fluids when the flow is not irrotational. *Proc. Roy. Soc. London*, **93A**, 99–113, https://doi.org/10.1098/rspa.1917.0007.

Thomson, R. E., and W. J. Emery, 2014: *Data Analysis Methods in Physical Oceanography*. 3rd ed., Elsevier, 728 pp.

Våge, S., S. L. Basedow, K. S. Tande, and M. Zhou, 2014: Physical structure of the Barents Sea Polar Front near Storbanken in August 2007. *J. Mar. Syst.*, **130**, 256–262, https://doi.org/10.1016/j.jmarsys.2011.11.019.

Venegas, S. A., and L. A. Mysak, 2000: Is there a dominant timescale of natural climate variability in the Arctic? *J. Climate*, **13**, 3412–3434, https://doi.org/10.1175/1520-0442(2000)013<3412:ITADTO>2.0.CO;2.

Wang, M., and J. E. Overland, 2012: A sea ice free summer Arctic within 30 years: An update from CMIP5 models. *Geophys. Res. Lett.*, **39**, L18501, https://doi.org/10.1029/2012GL052868.

Weatherall, P., and Coauthors, 2015: A new digital bathymetric model of the world's oceans. *Earth Space Sci.*, **2**, 331–345, https://doi.org/10.1002/2015EA000107.

Yang, J., and J. F. Price, 2000: Water-mass formation and potential vorticity balance in an abyssal ocean circulation. *J. Mar. Res.*, **58**, 789–808, https://doi.org/10.1357/002224000321358918.

Yang, X. Y., X. Yuan, and M. Ting, 2016: Dynamical link between the Barents-Kara sea ice and the arctic oscillation. *J. Climate*, **29**, 5103–5122, https://doi.org/10.1175/JCLI-D-15-0669.1.